Competing Crosstalk between Cytoskeletal Filaments Dictates Structure and Superdiffusivity of Microtubules in Live Cells

Renita Saldanha [1,2] Yiling Lan [2,3] Heidi Hehnly [2,3] Ryan J. McGorty [4]
Rae M. Robertson-Anderson [4] and Alison Patteson [1,2]

[1]*Physics Department, Syracuse University, Syracuse, New York 13244, USA*
[2]*BioInspired Institute, Syracuse University, Syracuse, New York 13244, USA*
[3]*Department of Biology, Syracuse University, Syracuse, New York 13244, USA*
[4]*Department of Physics and Biophysics, University of San Diego, San Diego, California 92110, USA*

(Received 19 January 2025; accepted 7 July 2025; published 5 August 2025)

The cytoskeleton is an active and complex composite network of actin, microtubules, and intermediate filaments (IFs). Networks of these distinct biopolymers work in partnership to fulfill fundamental cellular processes, such as cell polarization, intracellular transport, and cell migration. While there is evidence that the different cytoskeletal filaments interact through biochemical signaling and physical interactions, many basic questions remain regarding how this crosstalk impacts the dynamics and organization of the cytoskeletal filaments. Here, we combine Fourier image analysis methods with live cell experiments to characterize the impacts of cytoskeletal crosstalk on the structure and dynamics of microtubules in mouse embryonic fibroblasts. Specifically, we investigate the impacts of depleting vimentin IFs (vim $-/-$) as well as inhibiting actomyosin activity or inducing actin depolymerization. Using spatial image autocorrelation analysis, we identify that depleting vimentin decreases the effective mesh size of the microtubule network regardless of the state of the actin, while inhibiting myosin activity or depolymerizing actin increases the microtubule mesh size in cells with and without vimentin. Moreover, using differential dynamic microscopy, we reveal that microtubules exhibit superdiffusive motion over a wide range of length- and timescales, with rates that are enhanced in all cells lacking vimentin and suppressed in all cells where actin is disrupted. Our results reveal competing and seemingly independent roles that vimentin and actin play in mediating the dynamics and structure of the network of microtubules in cells across decades of spatiotemporal scales. We argue that these effects arise from the scaffolding ability of the vimentin and active dynamics of the actin, which independently sculpt microtubule network dynamics and structure in cells.

DOI: 10.1103/15vm-4d7b

I. INTRODUCTION

The mammalian cell cytoskeleton is a dynamic composite network of biopolymers, which is critical to many cellular features, including cell structure, organization, mechanical integrity, and migration [1,2]. The varied roles of the cytoskeleton are achieved by leveraging the properties of three different types of biopolymers: microtubules, actin filaments, and intermediate filaments (IFs) [3]. While all three filaments have comparable lengths, of the order of several microns, IFs are the most flexible, with a persistence length of $l_p \approx 1$ μm, compared to semiflexible actin filaments and rigid microtubules with $l_p \approx 10$ μm and $l_p \approx 1$ mm [2,4]. This broad range of stiffnesses enables distinct mechanical properties and functions [3]. For example, networks of vimentin IFs have been shown to exhibit strain stiffening behavior in response to shear and compressive strains, while actin filaments and microtubules have been shown to soften or rupture [1,2]. Microtubules play key roles in organelle transport [5], as well as cell polarization and migration [6], while actin regulates mechanosensing [7] and adhesion [8]. However, recent studies have demonstrated that vimentin also plays important roles in both migration [9] and mechanosensing [10,11]. These and other recent studies have highlighted the necessity of crosstalk between these three cytoskeletal filaments in sculpting the structural [12,13] and mechanical properties of the cell [1,14,15]. However, understanding the impact of this crosstalk on cell processes is hampered by the complexity of cell regulated biophysical properties and the large range of spatiotemporal scales over which they occur (∼100 nm–10 μm, subsecond to hours). Few experimental approaches are able to bridge this necessary range of length- and timescales while maintaining careful control over components in living cells.

Here, we investigate the role of crosstalk with vimentin and actin on the structure and dynamics of microtubules within mouse embryonic fibroblasts (mEFs). Microtubules in cells undergo dynamic growth and shrinkage due to the addition of GTP-tubulin dimers at the growing edge [16,17], along with post-translational modifications, such as acetylation [18]

and de-tyrosination [19], that reduce breakage and disassembly of the filaments [20]. Microtubule dynamics are also influenced by thermal fluctuations and ATP-driven activity, as well as actomyosin contractility [17,21–23]. Intermediate filaments, such as vimentin, form viscoelastic networks [24] that are suggested to suppress cytoplasmic dynamics [25] and microtubule buckling modes [26], yet the nature of this suppression and its impact on the cell-spanning network of microtubules is poorly understood and has important implications on polarization, migration, and cell-generated traction forces [27,28].

Here, by analyzing the spatial and temporal fluctuations of fluorescent-labeled microtubules in mEFs—with and without vimentin, actin filaments, and/or actomyosin activity—we elucidate the impact of cytoskeletal crosstalk on the dynamics and structure of the microtubule network in live cells across cell-spanning scales. Specifically, we use spatial image autocorrelation (SIA) and differential dynamic microscopy (DDM) to quantify the structural correlation lengthscales and transport properties of the network of microtubules [29–32]. Importantly, these methods extract information from raw images of microtubules without the need for tracking individual filaments, which is not possible at the high concentrations of microtubules found in cells and using imaging parameters that span the entire cell. These methods also do not rely on exogenous tracer particles, which may alter network structure and rely on assumptions that may be violated in cells to infer dynamics. While there are a number of recent studies that have investigated interactions between two of the three filament types [12,13,28], very few have examined three-way crosstalk [27,33], and none to our knowledge have explored whole cell network dynamics in live cells.

We find that microtubules display superdiffusive dynamics over several decades of spatiotemporal scales that are surprisingly robust to varying crosstalk conditions achieved by inducing actin depolymerization (using cytochalasin D) or inhibiting actomyosin activity (using blebbistatin in wild-type (vim + /+) and vimentin null (vim − /−) mEFs. However, the rate of motion, the structural correlation lengths, and their relative heterogeneity are tuned by the distinct crosstalk conditions. Moreover, we find that depleting vimentin both enhances the dynamics of the microtubule network and, counterintuitively, decreases its effective mesh size. In contrast, decreasing actomyosin activity or depolymerizing actin suppresses the dynamics of the microtubule network and increases the effective mesh size. Our study provides a systematic biophysical analysis without the need for specialized tools for understanding the intricate dynamics of the cytoskeleton at varying length- and timescales, and it reveals new insight into the complementary and competitive roles of cytoskeletal components in sculpting cytoskeletal structure and dynamics.

II. MATERIALS AND METHODS

A. Cell culture

Cells were maintained in Dulbecco's modified eagle's medium (DMEM) including HEPES and sodium pyruvate supplemented with 10% fetal bovine serum (FBS), 1% penicillin streptomycin, and nonessential amino acids (NEAA). Cell cultures were maintained at 37 °C with 5% CO_2.

B. Immunofluorescence

To analyze the cytoskeleton, cells were fixed using 100% methanol for 10 min at −20 °C. Cell membranes were permeabilized with 0.05% Triton-X in PBS for 15 min at room temperature and blocked with 1% bovine serum albumin (BSA) for 1 h at room temperature. For visualizing microtubules, we used primary alpha-tubulin rat antibody (Bio-rad) diluted 1:200 in 1% BSA in PBS for 1.5 h at room temperature and secondary antibody antirat Alexa Fluor 647 (Invitrogen) at a dilution of 1:1000 in 1% BSA in PBS for 1 h at room temperature. For visualizing vimentin, we used primary antivimentin rabbit antibody (Abcam) diluted in 1% BSA in PBS for 1.5 h at room temperature and secondary antirabbit Alexa Flour 488 (Invitrogen) at a dilution for 1:1000 in 1% BSA in PBS for 1 h at room temperature. For visualizing actin, the cells were fixed in 20% PFA (ThermoFischer) in PBS. The cell membranes were permeabilized with 0.05% triton-X in PBS for 15 min at room temperature and blocked with 1% BSA in PBS for 1 h at room temperature. Actin filaments were stained with rhodamine phalloidin 647 (Invitrogen) for 1 h at room temperature. Cells were mounted using Prolong diamond antifade mountant (Life Technologies). Multichannel images of size 2400 × 2400 square-pixels (133.12 μm × 133.12 μm) and an exposure time of 100 ms were acquired using a spinning disk confocal (Yokogawa CSU-W1) on an inverted Nikon Ti-E microscope with 100× oil immersion objective (1.49 NA) and Andor Zyla CMOS camera.

C. Inhibitor treatment

To remove actin stress fibers, we treated cells with 2 μM cytochalasin D to depolymerize actin filaments. To determine the effects of actomyosin activity on microtubule dynamics, we treated cells with 10 μM blebbistatin (Sigma Aldrich, B0560), a myosin II inhibitor. Cells were treated with reagents for 2 h before fixation or live imaging.

D. Live imaging

For live imaging of microtubules, cells were plated on 35 mm glass bottom MatTek dishes. The cells were treated with Sir-tubulin (Cytoskeleton, Inc cy-sc002) at a concentration of 1000 nM and incubated at 37 °C and 5% CO_2 for 1–2 h. Before imaging, the cells were washed once with 1X PBS and the medium was changed to an imaging medium (cell culture medium without phenol red) to avoid autofluorescence from Dulbecco's Modified Eagel's Medium (DMEM). Microtubules within the cells were imaged using Leica DMi8 STP800 equipped with an X-light V2 confocal unit spinning disk, 89 North-LDI laser launch, and 647 nm laser at 3% power. 1200 × 1200 pixel images were captured using an HC PL APO 63 × 1.4NA oil objective and Photometrics Prime-95B camera with an effective pixel size of 0.066 μm. VISIVIEW software was used to acquire 2000-frame videos at 6 fps (for a total time of ∼5.5 min) with an exposure time of 100 ms per frame. The cells were incubated at 37 °C and 5% CO_2

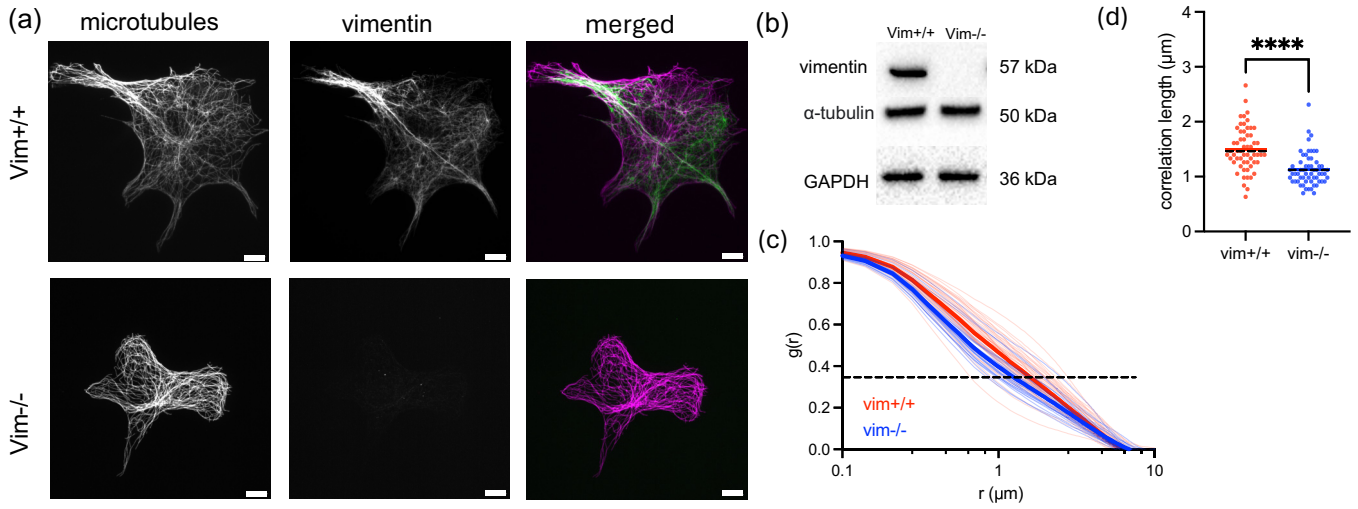

FIG. 1. Vimentin alters the structure of microtubule networks in cells. (a) Confocal microscopy images of microtubules (left) and vimentin (middle), as well as the merged image (right) showing microtubules (magenta) and vimentin (green) in vim + /+ (top row) and vim − /− (bottom row) mEFs. Scale bar for all images is 10 μm. (b) Western blot for vimentin, α-tubulin, and GAPDH (control) in vim + /+ and vim − /− mEFs. (c) SIA autocorrelation function $g(r)$ vs r computed for the microtubule channel for each imaged cell (faint lines) in vim + /+ (red) and vim − /− (blue) mEFs. Thick color-coded lines correspond to the average of the individual curves $\langle g(r)\rangle$ and the dotted line corresponds to the $g(r) = e^{-1}$, and its intersection with each curve denotes the corresponding correlation length ξ plotted in (d). (d) The correlation length ξ for vim + /+ (red) and vim − /− (blue) cells and its average denoted by the horizontal lines and the average value from the average curve in (c) is denoted by the dashed black line ($N = 50$ cells collected over $n = 2$ independent experiments).

during imaging. The frame rate was chosen to be fast enough to capture microtubule fluctuations, while still allowing for sufficient signal-to-noise, and the acquisition time was chosen to be short enough to prevent cell migration from causing detectable changes in the cell shape or position. The cells were incubated at 37 °C and 5% CO_2 during imaging.

E. Spatial image autocorrelation analysis

To analyze microtubule network structure, we use spatial image autocorrelation (SIA), as described before [31]. The autocorrelation function $g(r)$ measures the autocorrelation of pixel intensities in an image $I(r)$ as a function of separation distance Δr. To compute $g(r)$, we take the inverse Fourier transform F^{-1} of the product of the fast Fourier transform of the image $F(I)$ and its complex conjugate, which we normalize by the square of the intensity $I(r)$ to obtain the image autocorrelation function, $g(r) = \frac{F^{-1}\{F\{I(r)\}^2\}}{I(r)^2}$.

We compute $g(r)$ for each fixed sample (containing a single cell), and we average across all cells for each condition to obtain $\langle g(r)\rangle$. We quantify a characteristic structural correlation lengthscale ξ, which can be considered a measure of the effective mesh size of a network, by determining the distance at which $g(\xi) = e^{-1}$ for each cell. For the data presented in the manuscript, we use the full microtubule image. To check whether boundary effects impacted the result, we performed SIA with smaller subregions of the cell. See Fig. 1 of the Supplemental Material (SM) [34] for more details. We also computed $g(r) = 0.5$ (SM Fig. 2).

F. Differential dynamic microscopy

To quantify the dynamics of microtubule networks in cells, we performed differential dynamic microscopy (DDM) [29] on a 256 × 256 square-pixel (45 μm × 45 μm) region-of-interest (ROI) for each cell, chosen to capture >70% of the cell and remain fully contained within the cell. DDM calculates the squared Fourier transform of image differences $\Delta I(x, y, \Delta t) = I(x, y, t + \Delta t) - I(x, y, t)$ separated by varying lag times Δt, which is then radially averaged to give the image structure function $D(q, \Delta t)\langle|\Delta\tilde{I}(q, \Delta t)|^2\rangle_t$, where we define $q = 2\pi r^{-1}$ as the magnitude of the wave vector, and r is the lengthscale. Next, we obtained the density fluctuation decay time $\tau(q)$ by fitting the $D(q, \Delta t)$ to $D(q, \Delta t) = A(q)[1-f(q, \Delta t)] + B(q)$, where $A(q)$ is the amplitude, $B(q)$ is the background related to the noise in the image, $f(q, \Delta t) = \exp(-(\frac{\Delta t}{\tau(q)})^{s(q)})$ is the intermediate scattering function (ISF), and $s(q)$ is the stretching factor (SM Fig. 5) [35]. The parameters $A(q)$ and $B(q)$ are fit parameters obtained by fitting the DDM image structure function $D(q, \Delta t)$ to a stretched exponential model for the ISF.

G. Statistics

Data are presented as a mean value ± standard error of mean (SEM). Each experiment was performed at least three times for DDM analysis and two times for SIA analysis. For DDM analysis, we analyzed a total of 30 movies for each condition. For SIA, we analyzed a total of 60 cells per condition. The unpaired Student's t-test with 95% confidence level was used to determine statistical differences between distributions. Denotations: *, $p \leqslant 0.05$; **, $p \leqslant 0.01$; ***, $p \leqslant 0.001$; ****, $p \leqslant 0.0001$; n.s., $p > 0.05$. n and N represent, respectively, the number of independent experiments and sample size (number of cells or number of measurements) per condition. All the graphs and statistical analyses were done using GraphPad PRISM version 9 (GraphPad Software, Inc.).

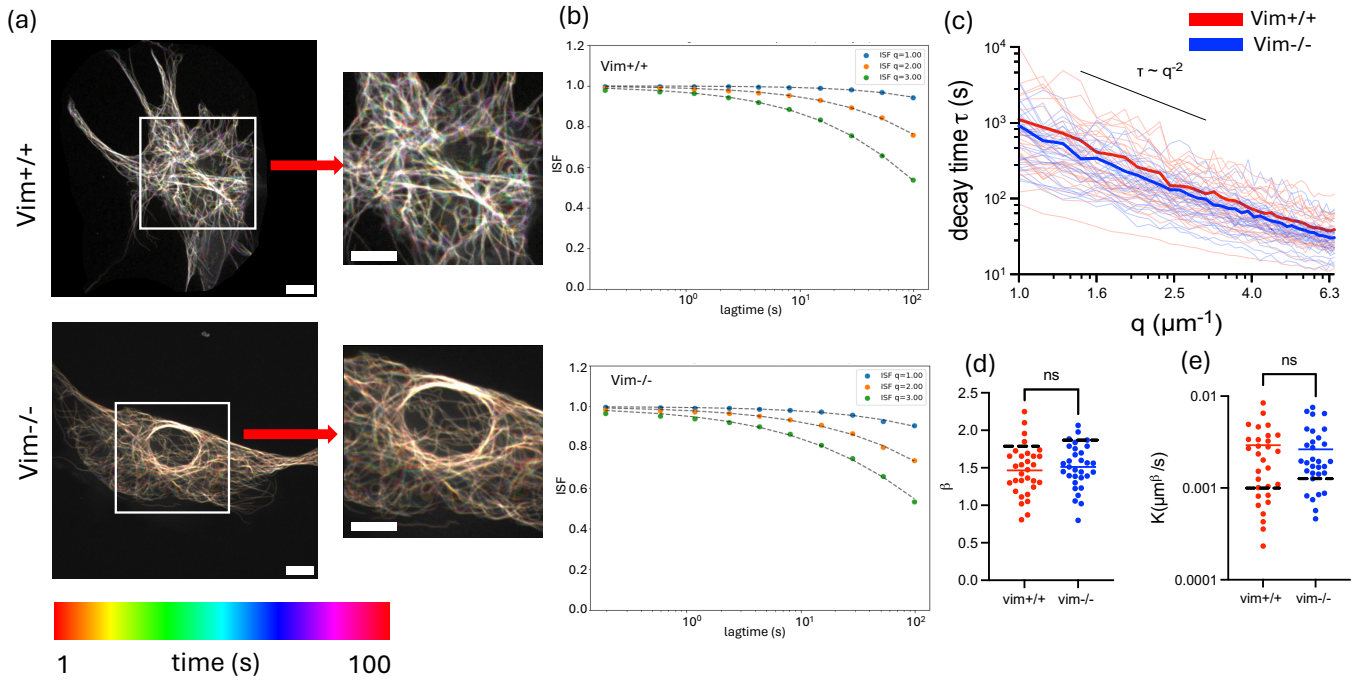

FIG. 2. Fluctuations of microtubules from live imaging videos and their spatial-temporal analysis. (a) Temporal color code images for vim + /+ and vim − /− mEF over 100 s. White pixels correlate with areas of little motion. Zoomed-in image of the microtubule network marked by a white box is indicated by red arrows. Scale bar for all images is 10 μm. (b) ISF vs lag time plots for vim + /+ and vim − /− mEFs, where the dots represent the data and the dotted lines represent the fits using the stretched exponential model. (c) Decay time τ vs wave vector q for vim +/+ (red) and vim − /− (blue) mEFs, where thin and thick lines correspond to individual cells and the average, respectively ($N = 32$ cells over $n = 3$ replicates). (d) The distribution of scaling exponents β (circles) determined from fits to the individual $\tau(q)$ curves shown in (b), and their average (horizontal line), plotted for vim + /+ (red) and vim − /− (blue) cells. The black dashed line indicates the scaling exponents β for the average line in (b). (e) The distribution of transport coefficients K (circles) determined from fits to the individual $\tau(q)$ curves shown in (b), and their average (horizontal line), plotted for vim + /+ (red) and vim − /− (blue) cells. The black dashed line indicates the transport coefficients K for the average line in (b).

III. RESULTS

A. Vimentin increases structural correlation lengths and heterogeneity of microtubule networks

To determine the effect of vimentin on the structure of the cytoskeletal microtubule network, we examine immunofluorescence images of mouse embryonic fibroblasts (mEFs) labeled with antitubulin and antivimentin antibodies to visualize microtubules and vimentin, respectively [Fig. 1(a)]. Qualitatively, we observe that microtubules in wild-type (vim + /+) and vimentin-null (vim − /−) mEFs adopt similar structures, but the microtubule network appears modestly more heterogeneous and bundled in vim + /+ cells. Western blots of vimentin, α-tubulin, and GAPDH in both cell types confirm that vimentin is knocked out in vim − /− cells and the microtubule concentration is unchanged, consistent with prior studies [25]. These prior studies also reported vim − /− cells to have similar actin concentrations [25] and structure [36] to wild-type cells. Thus, we expect the qualitative differences in the microtubule network structure to arise from the loss of interactions with vimentin.

To quantify the impact of vimentin on the microtubule network structure, we perform SIA on the microtubule immunofluorescence images, which computes the correlation in intensity between two pixels separated by distance r (see Methods). The resulting autocorrelation function $g(r)$ typically decays with increasing r, and a characteristic structural correlation length ξ can be estimated as $g(\xi) = e^{-1}$. Steeper/shallower decays indicate smaller/larger network features and correlation lengthscales, and for homogeneous networks, ξ can serve as a proxy for the mesh size. Figure 1(c) shows $g(r)$ curves computed for each imaged cell (faint lines) and the average across cells $\langle g(r)\rangle$ for wild-type and vimentin-null mEFs. While there is overlap in the spread of the data between the two cell types, vim + /+ cells exhibit a shallower decay of $\langle g(r)\rangle$ with distance and an increased spread in the ensemble of individual curves as compared to vim − /− cells. These features indicate that the microtubule network in the absence of vimentin is more homogeneous and has smaller structural features (e.g., mesh pores).

Evaluating the correlation length for each measured cell [Fig. 1(d)], we find that cells with vimentin have a higher average correlation length of $\langle\xi\rangle \simeq 1.5$ μm compared to $\langle\xi\rangle \simeq 1$μm for vimentin-null cells ($p < 0.0001$). We also observe a larger spread in individual ξ values, as shown by the larger spread in the data points for vim + /+ [Fig. 1(d)]. These quantitative analyses, which confirm the qualitative depiction [Fig. 1(a)], suggest that vimentin increases the average microtubule network mesh size and its associated spread by increasing filament bundling and/or other multifilament

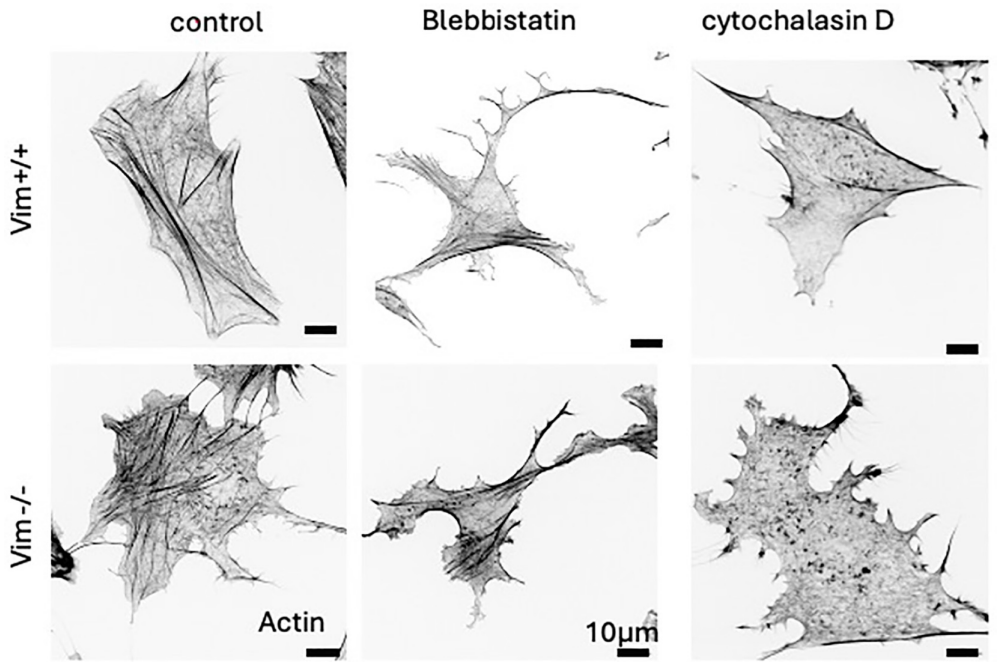

FIG. 3. Disrupting actomyosin activity and actin polymerization alter the structure of the actin cytoskeleton in wild-type and vimentin null cells. Actin network in vim + /+ (top row) and vim − /− (bottom row) mEF subject to three treatments: control (no inhibitors added, left), 10 μM blebbistatin (middle), and 2 μM cytochalasin D. Cells were fixed after 2 h exposure to inhibitors. Scale bar for all images is 10 μm.

structures that serve to increase the magnitude and heterogeneity of the spacing between distinct network fibers (i.e., bundles, multifilament structures, or individual filaments).

B. Microtubules exhibit superdiffusive motion in live cells

Based on prior work, which shows that vimentin dampens temporal fluctuations in the cell cytoplasm [25], we hypothesized that vimentin may slow the dynamics of microtubules in live cells. To test this hypothesis, we analyzed microtubule dynamics captured in videos of fluorescently labeled microtubules in live cells using differential dynamic microscopy (DDM) (Fig. 2) (see the SM and Methods).

Qualitative analysis of the videos suggests that there are larger microtubule fluctuations in the vimentin-null cells compared to the wild-type cells [Fig. 2(a)]. Specifically, Fig. 2(a) shows temporal color maps of sample vim + /+ and vim − /− videos, in which the different colors denote different points in time. Images with more color indicate more motion over the 100 s timescale of the video, whereas white pixels indicate no detected motion (all colors are overlapping). We observe significantly more color in vim − /− versus vim + /+, suggesting that the amplitude of microtubule motion is lower in the presence of vimentin.

To quantify the qualitatively evident impact of vimentin on microtubule dynamics, we performed DDM on cropped ROIs of the videos that are centered on and enclose >70% of the cell interior [Fig. 2(a)], as described in Methods. DDM yields characteristic density fluctuation decay times τ for varying wave numbers q from which we can determine the type and rate of motion of the microtubules. Specifically, the decay time typically exhibits power-law scaling with q of the form $\tau = K^{-1}q^{-\beta}$, where K is the generalized transport coefficient, which reduces to the diffusion coefficient for diffusive motion, and β is related to the anomalous scaling exponent $\alpha = 2\beta^{-1}$. The anomalous scaling exponent α occurs when the mean-squared displacement $\langle r^2(t)\rangle \sim t^{\alpha}$, where $\alpha < 1$ implies slower than linear growth due to constraints like crowding and $\alpha > 1$ suggests faster than linear growth like active transport. Thus, in the context of DDM, $\beta = 2$, $\beta > 2$, and $\beta < 2$ correspond to diffusive ($\alpha = 1$), subdiffusive ($\alpha < 1$), and superdiffusive ($\alpha > 1$) motion, respectively. As shown in Fig. 2(c), which shows $\tau(q)$ for individual cells (faint lines) and their average (dark lines), both vim + /+ and vim − /− mEFs exhibit similar power-law scaling and spread in the data across the entire q range, which corresponds to lengthscales that we define here as $\lambda = 2\pi q^{-1} \simeq 1 - 6\,\mu$m, spanning from below the mesh size to comparable to the lengths of microtubules. However, the magnitude of $\tau(q)$ is larger for vim + /+ compared to vim − /− mEFs, indicative of slower dynamics across the entire spatiotemporal range. This can be seen, for instance, by plotting the decay time for both cell types at a specific q value as done in SM Fig. 3. Figure 2(b) shows the ISF plots and SM Figs. 4 and 5 show the DDM matrix fit plot and stretching factor plots respectively for vim + /+ and vim − /− mEFs obtained by using the stretched exponential model.

Power-law fitting of the individual $\tau(q)$ curves shown in Fig. 2(c) yields the distribution of scaling exponents β [Fig. 2(d)] and transport coefficients K [Fig. 2(e)] for vim + /+ and vim − /− mEFs. We observe that both cell types have similar transport coefficients and scaling exponents, with an average scaling exponent of $\beta \approx 1.5$ indicative of superdiffusive motion. Superdiffusivity suggests active

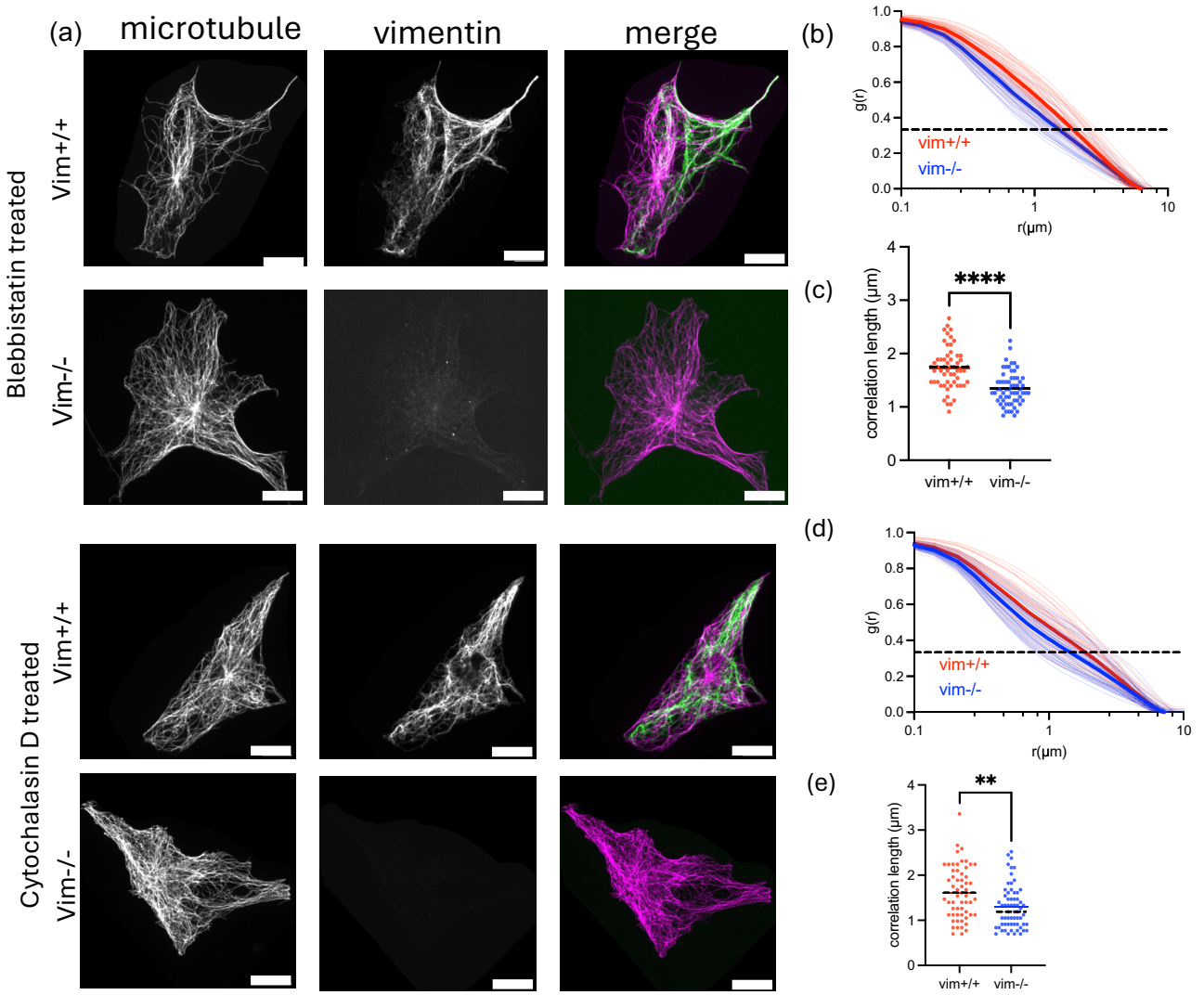

FIG. 4. Microtubule and vimentin network structure after treatment with inhibitors of myosin motor activity and F-actin polymerization. (a) Microtubules (left), vimentin (center), and merged network image in vim $+/+$ and vim $-/-$ mEF treated with blebbistatin (10 μM) (top two rows) and cytochalasin D (2 μM), respectively (bottom two rows). (b),(d) Spatial image autocorrelation function $g(r)$ vs r computed for microtubule channel in vim $+/+$ (red) and vim $-/-$ (blue) mEF treated with blebbistatin and cytochalasin D. Thick color-coded lines correspond to the average of the individual curves $\langle g(r)\rangle$ and the dotted line corresponds to $g(r) = e^{-1}$, and its intersection with each curve denotes the corresponding correlation length ξ plotted in (c) and (e). (c),(e) correlation length ξ for vim $+/+$ (red) and vim $-/-$ (blue) cells for blebbistatin and cytochalasin D treated cases, respectively, and its average denoted by the horizontal lines and the average value from the average curve in (b) and (d) denoted by the dashed black line ($N = 50$ cells collected over $n = 2$ independent experiments). All scale bars are 10 μm.

athermal transport, which has been reported for actin filaments in cells [37], presumably due to actomyosin activity, but is not obvious for microtubules. Our results are also at odds with reports that vimentin dampens microscale diffusive-like fluctuations of vesicles and individual buckling of microtubule fibers [23,25,27], which should manifest as higher and lower β and K values, respectively. However, the spread in both β and K values is larger for vim $+/+$ compared to vim $-/-$ cells, consistent with the larger spread in structural lengthscales [Fig. 1(d)]. This correlation suggests that the variation in transport properties of microtubules across the lengthscale of the cell is dictated by the structural heterogeneity. Moreover, the previously reported effects of vimentin on microtubule buckling and diffusive dynamics spanned much smaller lengthscales, suggesting these effects are localized and thus contribute to the heterogeneity but not the collective average dynamics of the microtubule network.

C. Microtubule network structure depends on both vimentin and actomyosin contractility

We next seek to understand how interactions with actin impact this crosstalk by disrupting actomyosin activity and actin polymerization in vim $+/+$ and vim $-/-$ mEFs. We use cytochalasin D [38] to depolymerize existing actin filaments and prevent stress fiber formation, and we use the myosin II inhibitor, blebbistatin [39], to block actomyosin activity and further inhibit stress fiber growth. The effects of

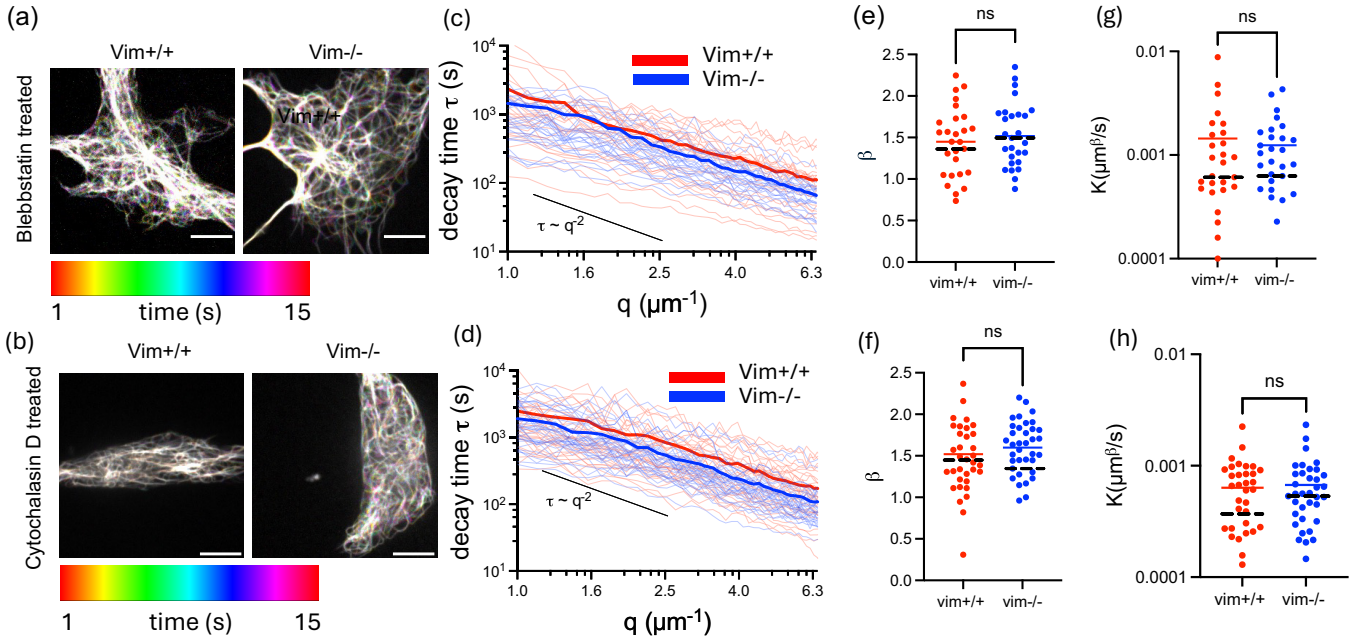

FIG. 5. DDM analysis of microtubule dynamics in live cells in the presence of actin inhibitors. (a),(b) Temporal color code images for vim + /+ and vim − /− mEF treated with blebbistatin and cytochalasin D respectively over 15 s. White pixels correlate with areas of little motion. (c),(d) Decay time τ vs wave vector plots for vim + /+ (red) and vim − /− (blue) mEFs for blebbistatin treated cells (10 μM) and cytochalasin D treated cells (2 μM), respectively, where thin and thick lines correspond to individual cells and the average, respectively. (e),(f) The distribution of β (circles) determined from fits to the individual $\tau(q)$ curves in (a) and (b), respectively, and their average horizontal line plotted for vim + /+ (red) and vim − /− (blue) cells for blebbistatin treated cells (10 μM) and cytochalasin D treated cells (2 μM), respectively. The dashed black line indicates the β value corresponding to the average (thick) line in (c) and (d), respectively. (g),(h) The distribution of transport coefficients K (circles) determined from fits to the individual $\tau(q)$ curves shown in (c) and (d), and their average (horizontal line), plotted for vim + /+ (red) and vim − /− (blue) cells treated with blebbistatin (10 μM) and cytochalasin D (2 μM), respectively. The dashed black line indicates the transport coefficient K value corresponding to the average (thick) line in (c) and (d), respectively ($N = 35$ cells collected over $n = 3$ experiments). All scale bars are 10 μm.

these inhibitors on actin network structure (gray scale image) are shown in Fig. 3 for wild-type and vimentin-null cells. As expected, the images show that the number and length of actin fibers are reduced by blebbistatin treatment, and cytochalasin D treatment essentially eliminates stress fibers and instead actin only appears to be present in the form of very small filaments or puncta.

To understand the role of these actin inhibition pathways on the structure of the microtubule network and the crosstalk with vimentin, we repeated the same immunofluorescence experiments shown in Fig. 1 for the actin-disrupted cases (Fig. 4). Images of the microtubules and vimentin in wild-type and vimentin-null mEFs show clear effects of actin disruption that depend on the presence of vimentin [Fig. 4(a)]. For example, blebbistatin-treated cells show largely separated networks of microtubules and vimentin, while the two networks are substantially more interpenetrating in cytochalasin-treated cells. Moreover, similar to the untreated cells [Fig. 1(a)], the microtubule network in the vim − /− cells appears more uniform with fewer bundles and voids.

SIA analysis on the microtubule networks in these experiments reveals similar behavior to the untreated case [Figs. 1(c) and 1(d)], with the average and distribution of $g(r)$ curves being higher for vim + /+ mEFs [Figs. 4(b) and 4(d)]. This result points to larger effective mesh sizes ξ in the vim + /+ case, as we find for untreated cells, and which we quantify by computing the correlation lengths for each $g(r)$ as well as its average [Figs. 4(c) and 4(e)]. For blebbistatin treated cells, we find that indeed ξ is larger for vim + /+ cells, with an average value of $\langle\xi\rangle \simeq 1.7$ μm compared to $\langle\xi\rangle \simeq 1.3$ μm for vim − /−. There is a similarly larger spread in the values for the vim + /+ case. These general trends hold for cytochalasin D cells, with average values of $\langle\xi\rangle \simeq 1.6$ μm and $\langle\xi\rangle \simeq 1.3$ μm for vim + /+ and vim − /− cells [Fig. 4(e)]. However, cytochalasin D treated cells exhibit a larger spread in the data for both cell types. Moreover, all measured correlation lengths are larger than those measured for untreated cells, indicating that actin reduces the microtubule mesh size in cells, perhaps due to microtubules being entrained in the contracting actomyosin network. This mechanism could also contribute to the superdiffusive dynamics we measure. The actin scaffold may also inhibit self-association and bundling of microtubules, which we see evidence for in the presence of vimentin, to decrease the mesh size.

D. Actin disruption slows microtubule dynamics without suppressing superdiffusivity

We next seek to determine how actin disruption impacts the microtubule dynamics with and without vimentin by

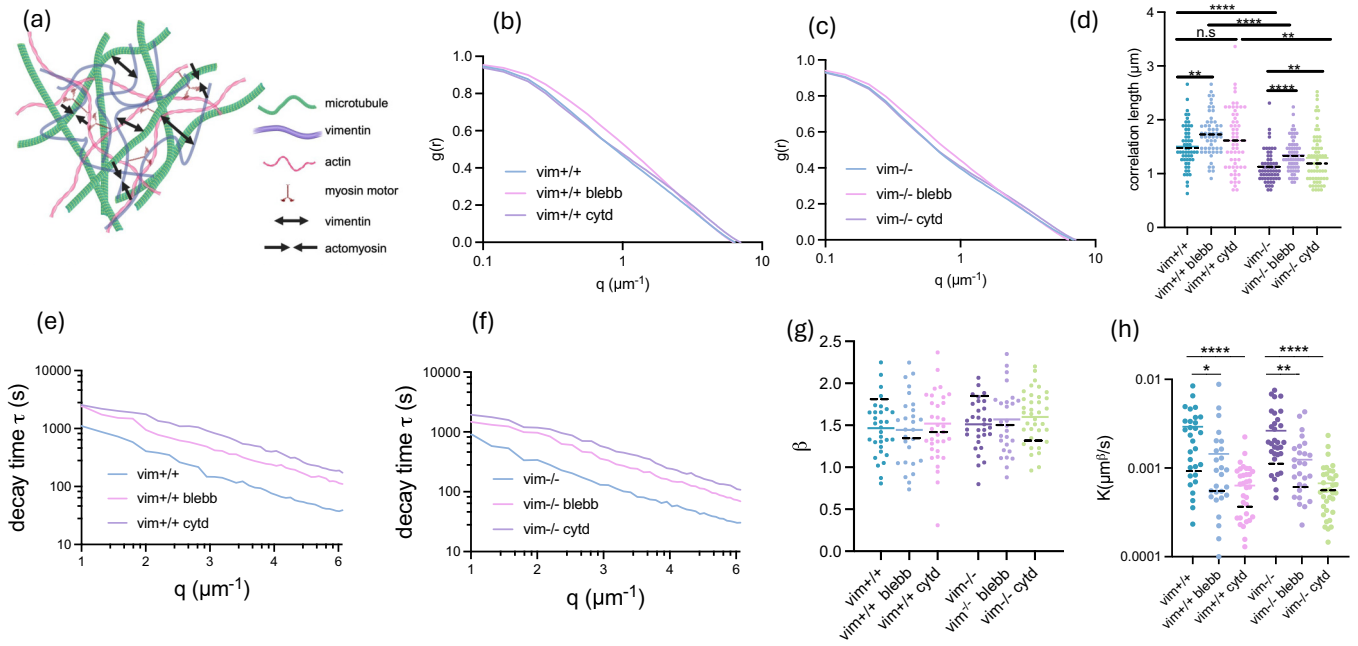

FIG. 6. Crosstalk with vimentin and actin dictates the structure and dynamics of microtubule networks in cells. (a) Schematic of cytoskeletal network in cells with the outward-pointing arrows indicating the pushing out of microtubules by vimentin and the inward-pointing arrows indicating the pulling inwards of microtubules by contracting actomyosin. (b),(c) Mean spatial image autocorrelation $\langle g(r)\rangle$ vs r for (b) vim $+/+$ and (c) vim $-/-$ cells that are untreated (blue), blebbistatin-treated (pink), or cytoD-treated (purple). (d) Individual correlation lengths ξ (circles) and their average (horizontal line) for treated and untreated vim $+/+$ (left) and vim $-/-$ (right) cells. (e),(f) Mean decay time τ vs wave vector q for (e) vim $+/+$ and (f) vim $-/-$ cells that are untreated (blue), blebbistatin-treated (pink), or cytoD-treated (purple). (g) Individual scaling exponents β (circles), their average (horizontal line), and β corresponding to the mean line in (e) and (f) (dashed black line) for treated and untreated vim $+/+$ (left) and vim $-/-$ (right) cells. (h) Individual transport coefficients K (circles), their average (horizontal line), and transport coefficient (K) corresponding to the mean line in (e) and (f) (dashed black line) for treated and untreated vim $+/+$ (left) and vim $-/-$ (right) cells.

performing similar live cell experiments and DDM analysis to that presented in Fig. 2. Figures 5(a) and 5(b) show the temporal color code images for blebbistatin and cytochalasin D treated vim $+/+$ and vim $-/-$ mEFs, respectively. In both blebbistatin and cytochalasin D treated cases, we observe more white pixels in vim $+/+$ cells which correspond to little motion compared to vim $-/-$ cells. As shown in Figs. 5(c) and 5(d), the average decay time $\tau(q)$ is slightly higher across all q values for vim $+/+$ cells for both treatments, indicating slower motion, similar to the untreated cases.

Moreover, power-law fits to the data reveal that microtubules undergo superdiffusive transport with similar scaling exponents to the control case, with average values of $\beta \approx 1.5$ and $\beta \approx 1.6$ for blebbistatin [Fig. 5(e)] and cytoD [Fig. 5(f)] treated cells, respectively. The scaling exponents are also slightly higher (more superdiffusive) for vim $-/-$ compared to vim $+/+$ cells, an effect that is more pronounced for cytoD treated cells and in line with their lower $\tau(q)$ curves compared to vim $+/+$. Actin disruption does not appear to significantly impact the role of vimentin on transport coefficients, with K values for vim $+/+$ and vim $-/-$ mEFs similar for both types of actin treatments [Figs. 5(g) and 5(h)]. However, we do find that the type of actin disruption plays an important role in microtubule transport rates, with average values of $\langle K\rangle \approx 1\times10^{-3}\,\mu\text{m}^{-1.5}\,\text{s}^{-1}$ and $\langle K\rangle \approx 6\times10^{-4}\,\mu\text{m}^{-1.6}\,\text{s}^{-1}$ for blebbistatin and cytoD treated cells [Figs. 5(e) and 5(f)]. Thus, depolymerizing actin has a greater effect in suppressing microtubule dynamics compared to inhibition of myosin II motors.

IV. DISCUSSION AND CONCLUSIONS

Our results presented above demonstrate the complex and subtle ways in which crosstalk and interaction between the three key cytoskeletal polymers—microtubules, vimentin, and actin—dictate cytoskeletal structure and dynamics. We conjecture that the effects of vimentin and actin disruption on microtubules, summarized in Fig. 6, are a direct consequence of the cell's ability to carefully and dynamically balance mechanical rigidity and activity to achieve wide-ranging processes such as mechano-memory, motility, and polarization.

Specifically, Figs. 6(b)–6(d) show that microtubule correlation lengths are primarily controlled by vimentin, with vim $+/+$ cells having larger ξ values and spread among individual values than vim $-/-$, regardless of the state of the actin. This increase may arise from vimentin acting as a space-filling and interpenetrating network that effectively "pushes out" the microtubule network and drives filament bundling via depletion interaction to increase correlation lengths [Fig. 6(a)], consistent with prior microtubule-vimentin interaction studies [40].

Secondarily, we find modestly larger ξ values for blebbistatin treated compared to untreated cells, indicating that

actomyosin activity serves to reduce the microtubule mesh size by entraining the microtubules in the contracting network. This physical picture is consistent with previous work that points to the role of actomyosin forces in subjecting microtubule networks to compressive forces, which work together to set cellular traction forces [27]. Our data suggest that small microtubule mesh sizes are a signature of increased actomyosin activity, which could be an influential factor in setting cell stress.

We also observe a larger spread in values for the cytoD treated cells compared to the other cases, suggesting that the network of actin filaments may play an important role in reducing structural heterogeneity of microtubules by providing an interpenetrating stress-bearing scaffold. Disrupting myosin via blebbistatin would primarily suppress actomyosin activity without appreciably altering the actin scaffold, so the effect on heterogeneity should be much less pronounced, as we observe.

Intuitively, one may expect increased or decreased mesh sizes to lead to increased or decreased transport, as a larger mesh size implies fewer steric constraints (i.e., entanglements) with surrounding filaments and larger network voids which both allow for less restricted filament motion. However, we find much more complex behavior [Figs. 6(e)–6(h), and SM Fig. 4]. Namely, actin disruption slows microtubule dynamics similarly for both vim $+/+$ and vim $-/-$ cells, with cytoD having a more pronounced effect. The role of vimentin on transport is much weaker, with vim $+/+$ cells exhibiting more spread in K and β values for all cases with relatively little effect on their magnitudes.

Despite these differences, microtubules exhibit robust superdiffusive dynamics for all cell types and treatment over the entire spatiotemporal range of our measurements. We highlight here that there is no *a priori* expectation that the dynamics should be superdiffusive given the complexity of the cytoskeletal system [41]. Prior studies have found diffusive dynamics for tracer particles inside the cell and microtubule filaments in reconstituted networks [25]. Microtubule fluctuations are driven in large part by ATP-activity in the cell, which can drive buckling of microtubule filaments within the cell [26]. On the other hand, buckling and fluctuations of microtubules are also coupled to the local mechanical and structural properties of the cell cytoskeleton. It has been reported that the surrounding elasticity and network of the cytoskeletal polymers dampen microtubules fluctuations [26,42], consistent with the modestly increased transport in vimentin-null cells [Fig. 6(g)]. On the other hand, one could reason that the superdiffusive behavior arises because the microtubules are embedded in a viscoelastic medium with a strong frequency dependence [25].

In conclusion, our work sheds important new light on the role of crosstalk between cytoskeletal filaments in the network structure and dynamics. This is essential to understanding many biophysical aspects of the cell, including mechanical properties, motility, and polarization. We quantified the structure and dynamics of *in vivo* microtubule networks using spatial and temporal correlation functions from statistical physics to analyze immunofluorescence and video data. Our methodology demonstrates how to measure physiologically relevant parameters of cytoskeletal structure and dynamics that can be employed with other techniques to understand multiscale cytoskeletal and cellular functions.

In future studies, it would be interesting to combine these approaches with other techniques for greater detail of cytoskeletal structure and dynamics. One technical limitation is the two-dimensional nature of our study. Possible parallel approaches include fluorescence recovery after photobleaching (FRAP) [43], microrheology [44,45], microtubule buckling analysis [46], fluorescently labeled microtubule tip binding proteins [47], and quantitative protein analysis. The statistical physics approaches used in this manuscript could also be combined with approaches from thermodynamics to understand the biophysical properties of the cytoskeleton. We speculate that there is a hidden cytoskeletal order that can be quantified with statistical physics approaches, and this order is integral to balancing the myriad entropic and dissipative processes that dominate cell processes.

ACKNOWLEDGMENTS

We thank Christoph Schmidt for insightful discussion. A.P. acknowledges support from NIH R35GM142963. R.A. and R.J.M. acknowledge NIH R15GM123420-02. H.H. acknowledges R01GM-127621 and R01GM-130874. Wild-type (vim $+/+$), vimentin-null (vim $-/-$) mouse embryonic fibroblasts were kindly provided by J. Ericsson (Abo Akademi University, Turku, Finland).

R.S. performed experiments and analysis, interpreted data, and wrote the manuscript; Y.L. helped with acquiring time lapse videos, H.H. provided experimental insights; R.J.M. provided software, guided analysis, interpreted data, and edited the manuscript; R.A. provided software, guided experiments and analysis, interpreted data, and wrote the manuscript; A.P. designed and supervised the research, guided experiments and analysis, interpreted data, and wrote the manuscript.

The authors declare no competing interests.

DATA AVAILABILITY

The data that support the findings of this article are not publicly available. The data are available from the authors upon reasonable request.

[1] K. Pogoda *et al.*, Unique role of vimentin networks in compression stiffening of cells and protection of nuclei from compressive stress, Nano Lett. **22**, 4725 (2022).

[2] A. E. Patteson *et al.*, The vimentin cytoskeleton: When polymer physics meets cell biology, Phys. Biol. **18**, 011001 (2020).

[3] A. F. Pegoraro, P. Janmey, and D. A. Weitz, Mechanical properties of the cytoskeleton and cells, Cold Spring Harb. Perspect. Biol. **9**, a022038 (2017).

[4] C. Hookway *et al.*, Microtubule-dependent transport and dynamics of vimentin intermediate filaments, Mol. Biol. Cell **26**, 1675 (2015).

[5] I. M. Kulić *et al.*, The role of microtubule movement in bidirectional organelle transport, Proc. Natl. Acad. Sci. **105**, 10011 (2008).

[6] S. Etienne-Manneville, Microtubules in cell migration, Annu. Rev. Cell Dev. Biol. **29**, 471 (2013).

[7] D.-H. Kim *et al.*, Actin cap associated focal adhesions and their distinct role in cellular mechanosensing, Sci. Rep. **2**, 555 (2012).

[8] A. I. Bachir, A. R. Horwitz, W. J. Nelson, and J. M. Bianchini, Actin-based adhesion modules mediate cell interactions with the extracellular matrix and neighboring cells, Cold Spring Harb. Perspect. Biol. **9**, a023234 (2017).

[9] F. Huber *et al.*, Cytoskeletal crosstalk: When three different personalities team up, Curr. Opin. Cell Biol. **32**, 39 (2015).

[10] M. Swoger *et al.*, Vimentin intermediate filaments mediate cell morphology on viscoelastic substrates, ACS Appl. Bio Mater. **5**, 552 (2022).

[11] A. E. Patteson, Loss of vimentin enhances cell motility through small confining spaces, Small **15**, 1903180 (2019).

[12] H. Wu *et al.*, Vimentin intermediate filaments and filamentous actin form unexpected interpenetrating networks that redefine the cell cortex, Proc. Natl. Acad. Sci. USA **119**, e2115217119 (2021).

[13] L. Pradeau-Phélut and S. Etienne-Manneville, Cytoskeletal crosstalk: A focus on intermediate filaments, Curr. Opin. Cell Biol. **87**, 102325 (2024).

[14] T. Hohmann and F. Dehghani, The cytoskeleton—a complex interacting meshwork, Cells **8**, 362 (2019).

[15] A. Oberhofer *et al.*, Molecular underpinnings of cytoskeletal cross-talk, Proc. Natl. Acad. Sci. USA **117**, 3944 (2020).

[16] G. J. Brouhard and L. M. Rice, Microtubule dynamics: An interplay of biochemistry and mechanics, Nat. Rev. Mol. Cell Biol. **19**, 451 (2018).

[17] E. C. Ory *et al.*, Analysis of microtubule growth dynamics arising from altered actin network structure and contractility in breast tumor cells, Phys. Biol. **14**, 026005 (2017).

[18] D. Wloga, E. Joachimiak, and H. Fabczak, Tubulin post-translational modifications and microtubule dynamics, Int. J. Mol. Sci. **18**, 2207 (2017).

[19] K. Lavrsen *et al.*, Microtubule detyrosination drives symmetry breaking to polarize cells for directed cell migration, Proc. Natl. Acad. Sci. USA **120**, e2300322120 (2023).

[20] L. Eshun-Wilson *et al.*, Effects of α-tubulin acetylation on microtubule structure and stability, Proc. Natl. Acad. Sci. USA **116**, 10366 (2019).

[21] S. Li, C. Wang, and P. Nithiarasu, Effects of the cross-linkers on the buckling of microtubules in cells, J. Biomech. **72**, 167 (2018).

[22] M. Kikumoto *et al.*, Flexural rigidity of individual microtubules measured by a buckling force with optical traps, Biophys. J. **90**, 1687 (2006).

[23] C. Pallavicini *et al.*, Characterization of microtubule buckling in living cells, Eur. Biophys. J. **46**, 581 (2017).

[24] P. A. Janmey *et al.*, Viscoelastic properties of vimentin compared with other filamentous biopolymer networks, J. Cell Biol. **113**, 155 (1991).

[25] M. Guo *et al.*, The role of vimentin intermediate filaments in cortical and cytoplasmic mechanics, Biophys. J. **105**, 1562 (2013).

[26] C. P. Brangwynne *et al.*, Microtubules can bear enhanced compressive loads in living cells because of lateral reinforcement, J. Cell Biol. **173**, 733 (2006).

[27] F. Alisafaei *et al.*, Vimentin is a key regulator of cell mechanosensing through opposite actions on actomyosin and microtubule networks, Commun. Biol. **7**, 658 (2024).

[28] R. Saldanha, M. Tri Ho Thanh, N. Krishnan, H. Hehnly, and A. Patteson, Vimentin supports cell polarization by enhancing centrosome function and microtubule acetylation, J. R. Soc. Interface **21**, 20230641 (2024).

[29] H. N. Verwei, G. Lee, G. Leech, I. I. Petitjean, G. H. Koenderink, R. M. Robertson-Anderson, and R. J. McGorty, Quantifying cytoskeleton dynamics using differential dynamic microscopy, J. Vis. Exp. e63931 (2022).

[30] G. Lee *et al.*, Myosin-driven actin-microtubule networks exhibit self-organized contractile dynamics, Sci. Adv. **7**, eabe4334 (2021).

[31] G. Lee *et al.*, Active cytoskeletal composites display emergent tunable contractility and restructuring, Soft Matter **17**, 10765 (2021).

[32] J. Cho, R. Cerbino, and I. Bischofberger, Emergence of multiscale dynamics in colloidal gels, Phys. Rev. Lett. **124**, 088005 (2020).

[33] A. Robert *et al.*, Microtubule-dependent transport of vimentin filament precursors is regulated by actin and by the concerted action of Rho- and p21-activated kinases, FASEB J. **28**, 2879 (2014).

[34] See Supplemental Material at http://link.aps.org/supplemental/10.1103/15vm-4d7b for additional SIA data for small ROI and $g(r) = 0.5$ and DDM data for distribution of decay time for a given q value, DDM matrix fit and stretching coefficient from the DDM fit model.

[35] J. Alvarado, L. Cipelletti, and G. H. Koenderink, Uncovering the dynamic precursors to motor-driven contraction of active gels, Soft Matter **15**, 8552 (2019).

[36] A. E. Patteson *et al.*, Vimentin protects cells against nuclear rupture and DNA damage during migration, J. Cell Biol. **218**, 4079 (2019).

[37] V. Sposini *et al.*, Towards a robust criterion of anomalous diffusion, Commun. Phys. **5**, 305 (2022).

[38] J. F. Casella, M. D. Flanagan, and S. Lin, Cytochalasin D inhibits actin polymerization and induces depolymerization of actin filaments formed during platelet shape change, Nature (London) **293**, 302 (1981).

[39] M. Kovács *et al.*, Mechanism of blebbistatin inhibition of myosin II, J. Biol. Chem. **279**, 35557 (2004).

[40] Z. Gan *et al.*, Vimentin intermediate filaments template microtubule networks to enhance persistence in cell polarity and directed migration, Cell Syst. **3**, 252 (2016).

[41] C. P. Brangwynne, F. C. MacKintosh, and D. A. Weitz, Force fluctuations and polymerization dynamics of intracellular microtubules, Proc. Natl. Acad. Sci. USA **104**, 16128 (2007).

[42] M. Guo *et al.*, Probing the stochastic, motor-driven properties of the cytoplasm using force spectrum microscopy, Cell **158**, 822 (2014).

[43] K. Edson *et al.*, FRAP analysis of the stability of the microtubule population the neurites of chick sensory neurons, Cell Motil. Cytoskeleton **25**, 59 (1993).

[44] V. Pelletier *et al.*, Microrheology of microtubule solutions and actin-microtubule composite networks, Phys. Rev. Lett. **102**, 188303 (2009).

[45] Y. Li, X. Zhuang, and F. Niu, Quantitative investigation of the link between actin cytoskeleton dynamics and cellular behavior, Micromachines **13**, 1885 (2022).

[46] I. A. Schaap *et al.*, Elastic response, buckling, and instability of microtubules under radial indentation, Biophys. J. **91**, 1521 (2006).

[47] S. P. Maurer *et al.*, EB1 accelerates two conformational transitions important for microtubule maturation and dynamics, Curr. Biol. **24**, 372 (2014).